Original papers
Nanostructured, nanoscale materials and nanodevices

УДК 54.057:544.6.018 DOI: 10.17277/jamt.2023.01.pp.008-019

Galvanic synthesis of ZnO and ZnO(Al) coatings from dimethylsulfoxide electrolytic baths

© Natalia A. Martynova[a], Leonid S. Lepnev[b], Dmitry M. Tsymbarenko[a], Konstantin I. Maslakov[a], Tatyana B. Shatalova[a], Serguei V. Savilov[a], Anastasia V. Grigorieva[a] ✉

[a] *Lomonosov Moscow State University, Bld. 3, 1, Leninskie gory, Moscow, 119991, Russian Federation,*
[b] *P.N. Lebedev Physical Institute of the RAS, 53, Leninskiy pr., Moscow, 119991, Russian Federation*

✉ anastasia@inorg.chem.msu.ru

Abstract: Electrochemical formation of transparent semiconductive oxide (TSO) coatings based on zincite is an attractive, versatile and easily scalable method,which is promising for optoelectronics and chemical sensors. The complexity of the formation of zinc oxide and doped compounds such as ZnO(Al) coatings by electrochemical co-precipitation of zinc and aluminum compounds in aqueous media is connected with both different redox potentials of two metals and the formation of galvanic precipitates of significantly hydrated zinc and aluminum oxides. Application of non-aqueous media for zinc electrolytes can form a bimetallic deposit for the following gently oxidation to oxide (AZO). In the present study, dimethylsulfoxide (DMSO) is applied as a solvent. It is shown that the specifics of nucleation of zincite phase in DMSO electrolytes results in more porous coatings in comparison to the processes in aqueous plating solutions. Here, compositions of non-aqueous electrolytes and corresponding deposition potentials in potentiostatic mode have been optimized. The correlations of microstructure and elemental composition of the coatings with parameters of galvanic process have been studied. The presence aluminum at the surface of the samples in two different valent states have been shown using X-ray photoelectron spectroscopy. This is the result of the deficiency of wurtzite structure and the presence of γ-Al_2O_3 phases, most likely, resulted from segregation. It is shown that the developed synthesis method is promising for direct synthesis of porous coatings of zincite with a variable deficiency of the structure.

Keywords: zinc oxide; aluminum; transparent conductive coatings;porous coatings; electroplating, dimethylsulfoxide; micromorphology; elemental composition; energy-dispersive X-ray spectroscopy; X-ray photoelectron spectroscopy.

For citation: Martynova NA, Lepnev LS, Tsymbarenko DM, Maslakov KI, Shatalova TB, Savilov SV, Grigorieva AV. Galvanic synthesis of ZnO and ZnO(Al) coatings from dimethylsulfoxide electrolytic baths. *Journal of Advanced Materials and Technologies*. 2023;8(1):008-019. DOI:10.17277/jamt.2023.01.pp.008-019

Гальваническое формирование покрытий ZnO и ZnO(Al) с использованием электролитов на основе диметилсульфоксида

© Н. А. Мартынова[a], Л. С. Лепнев[b], Д. М. Цымбаренко[a], К. И. Маслаков[a], Т. Б. Шаталова[a], С. В. Савилов[a], А. В. Григорьева[a] ✉

[a] *Московский государственный университет имени М. В. Ломоносова (МГУ), Ленинские горы, д. 1, стр. 3, Москва, 119991, Российская Федерация,*
[b] *Физический институт имени П. Н. Лебедева РАН, Ленинский проспект, д. 53, Москва, 119991, Российская Федерация*

✉ anastasia@inorg.chem.msu.ru

Аннотация: Электрохимическое формирование покрытий прозрачных полупроводниковых оксидов на основе цинкита – привлекательный универсальный и легкомасштабируемый метод, который является многообещающим для оптоэлектроники и химических сенсоров. Сложность в формировании покрытий на основе оксида цинка и легированных составов, таких как ZnO(Al), путем электрохимического соосаждения производных цинка

и алюминия в водных средах связана с различием окислительно-восстановительных потенциалов двух металлов и формированием гальванических осадков гидратированных оксидов цинка и алюминия. Применение неводных сред в роли электролитов цинкования может позволить сформировать биметаллический осадок для последующего контролируемого окисления до оксида (AZO). В рамках данной статьи в роли растворителя выступал диметилсульфоксид (ДМСО). Показано, что особенности нуклеации и роста фазы цинкита в электролитах на основе ДМСО приводят к образованию значительно более пористых покрытий металлического цинка, окисляемого в дальнейшем до цинкита, по сравнению с процессами вводных электролитах. Оптимизированы составы неводных электролитов и потенциалы формирования пленок в потенциостатическом режиме. Изучены корреляции микроструктуры и элементного состава от условий протекания гальванического процесса. Методом рентгеновской фотоэлектронной спектроскопии показано присутствие алюминия на поверхности образцов в двух различных валентных состояниях, что может быть следствием дефектности структуры вюрцита и присутствием фазы γ-Al_2O_3 – вероятного продукта сегрегации. Показано, что предложенный синтетический подход может быть перспективен для направленного формирования пористых тонкостенных покрытий цинкита с варьируемой степенью дефектности структуры.

Ключевые слова: оксид цинка; алюминий; прозрачные проводящие покрытия; пористые покрытия; электроосаждение, диметилсульфоксид; микроструктура; элементный состав; рентгеноспектральный микроанализ; рентгеновская фотоэлектронная спектроскопия.

Для цитирования: Martynova NA, Lepnev LS, Tsymbarenko DM, Maslakov KI, Shatalova TB, Savilov SV, Grigorieva AV. Galvanic synthesis of ZnO and ZnO(Al) coatings from dimethylsulfoxide electrolytic baths. *Journal of Advanced Materials and Technologies*. 2023;8(1):008-019. DOI:10.17277/jamt.2023.01.pp.008-019

1. Introduction

A new synthesis method for Al-doped ZnO coatings (ZnO(Al), AZO) with the required conductivity and transparency, compact or with developed surface, with good adhesion and also mechanically strong is a difficult challenge for researchers working on new light-emitting diodes (LED) [1], photovoltaics (PV) [2–5], resistive gas sensors [6, 7], photocatalytic reactors [8, 9], fuel cells [10], etc. Electrochemical synthesis of ZnO films, and the more Al-doped ZnO films using aqueous and non-aqueous baths is a growing field which might be scrutinized in detail. Obviously, the electroplating provides precise control of some geometric parameters of precipitate including film thickness and average particle size controlling both nucleation and crystal growth rate. On the other hand, the resulting crystallinity and porosity of the coatings are varying with parameters, for instance, if use aqueous or non-aqueous electrolytic baths [11].

According to the literature, metal zinc coatings can be obtained by electroplating from aqueous or non-aqueous electrolytes. Generally, when an aqueous electrolyte is applied, lower current efficiency is observed which is caused by hydrogen production in the over-potential [12]. Also, $Zn(OH)_2$ is formed competing with ZnO oxide formation during electrodeposition in aqueous electrolytes. Non-aqueous electrolytes do not produce hydroxide anions, and so higher quality of Zn coatings is expected [13]. To decrease porosity and delamination of electrochemically formed coatings of zincite here we present the Zn and Al electrolytic baths based on dimethylsulfoxide (DMSO) which are to avoid formation hydrogen bubbles on the cathode.

It is noticeable that only in a few works the development of ZnO coatings has been performed by electrochemical deposition of zinc compounds from non-aqueous electrolytic baths [12–16]. The established results concerning the optimal grain size, film thickness and resulting composition are not detailed for non-aqueous electrolytic baths or contradict each other [16–18]. Riveros et al. [16] discuss the specifics of nucleation of zinc from DMSO electrolytic baths.

For electrochemical synthesis of AZO coatings Kang et al. [17] used zinc nitrate as a precursor and DMSO as a solvent for (001) oriented films of ZnO nanorods. Within non-aqueous baths, DMSO is a very useful solvent in fabricating metals due to its high dielectric constant, excellent solvating capacity and low toxicity. Since in aqueous electrolytes the formation of hydroxides of both zinc and aluminum is observed [12, 14], this paper proposes a group of new non-aqueous electrolytes for co-precipitation of zinc and aluminum at the cathode with the following oxidation by molecular oxygen on sintering.

2. Materials and Methods

2.1. Materials

ZnO and ZnO(Al) coatings were prepared by electrochemical plating of zinc in its DMSO solution, the process was carried out in a three-electrode cell at room temperature. The working and counter electrodes were placed parallel to each other and

separated by a distance of 2 cm. Composition of electrolyte was following: 0.2 M $Zn(CH_3COO)_2$–$2H_2O$ (dihydrate, purum, "Chimmed"), $Al(NO_3)_3$–$9H_2O$ (nonahydrate, purum, "Chimmed"), 0.05 M hydrogen peroxide H_2O_2 (p.a., 33 %, "Spectrum-Chim") and 0.5 M KNO_3 (unhydrous, purum, "Reachim") in DMSO (99.9 % CAS 67-68-5) solution. The reference electrode was a saturated aqueous Ag/AgCl electrode [12]. A platinum wire of 0.5 mm diameter was applied as a counter electrode. All films obtained were deposited in potentiostatic mode at –1.6 V while for the samples of 0 mol. % of Al the deposition potential was varied to minimize the crystallite growth rate.

2.2. The deposition of ZnO *and* ZnO(Al) *coatings*

Experiments for the deposition of ZnO and ZnO(Al) coatings were carried out using conductive transparent ITO substrates to examine microstructure and composition for further application as photoanodes. Potentiostat-galvanostat P-45X with IR compensation (Electrochemical Instruments, Russia) was applied for electrochemical experiments. The corresponding cyclic voltammetry (CV) curves and preferred electroplating modes are shown in Fig. 1 and Table 1. For the Al-doped samples formation a non-aqueous acetate zinc electrolyte with the addition of aluminum nitrate was chosen because of its higher solubility in DMSO in comparison with aluminum chloride and acetate. A number of samples with a theoretical ratio (Al/Zn)·100 % of 1, 2, 4, 6, 8 and 10 % were synthesized in two series at –1.6 V (Al-0, etc.) and –1.4 V (Al-0', etc.), respectively. In comparison to the coatings deposited from aqueous zinc electrolytes [12] the obtained samples contained

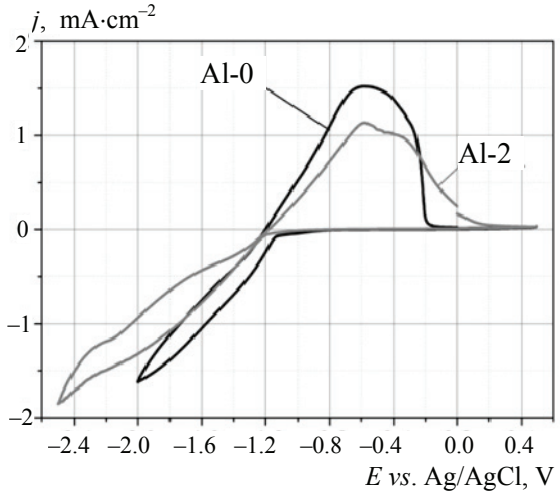

Fig. 1. Cyclic voltammograms of ITO electrode in DMSO acetate electrolyte for ZnO(Al) deposition. Scan rate – 50 $mV \cdot s^{-1}$

crystalline zinc oxide only but the samples were sintered at 500 °C for 1 hour in air to remove adsorbates.

2.3. Analytic methods

The sample morphologies of ZnO coatings were examined with a Leo Supra 50 VP (Carl Zeiss, Germany) scanning electron microscope and a Carl Zeiss NVision 40 (Carl Zeiss, Germany) scanning electron microscope (SEM) equipped with EDX Oxford Instruments X-MAX attachments for the local chemical analysis.

The TG-DTA analysis was performed with preliminary delaminated pristine coverages of complex composition using STA 409 PC Luxx coupled with a quadrupole mass spectrometer QMS 403C Aëolos (NETZSCH, Germany). Annealing was done in argon as a gas carrier with a flow rate of 30 $mL \cdot min^{-1}$. The samples were delaminated and then annealed up to 800 °C with a heating rate of 5 °/min and an isotherm at 800 °C for 30 min.

The GIXRD characterization of thin films was performed using Rigaku (Rigaku, Japan) SmartLab diffractometer equipped by 9 kW rotating Cu anode and Goebel mirror for parallel beam. Grazing incident geometry (omega = 0.5°) was appliedwith parallel slit analyzer of 0.5° on diffracted beam.

The X-ray photoelectron spectroscopy (XPS) data were acquired on an Axis Ultra DLD spectrometer (Kratos Analytical, UK) with a monochromatic AlK_α radiation source (hν = 1486.7 eV, 150 W). The pass energies of the analyser were 160 eV for survey spectra and 40 eV for high resolution scans. The charge neutralizer system was not used, but because of the slight charge of the sample surface during analysis the spectra were charge-corrected to give the C1s peak a binding energy of 285.0 eV.

Photoemission spectra were obtained using a multichannel spectrometer S2000 (Ocean Optics, USA) with a nitrogen laser LGI-21 (λ_{ex} = 337 nm) as an excitation source at 77 K. All spectra are corrected for the wavelength response of the system.

3. Results and Discussion

The characteristic CV curves obtained for zinc andzinc-aluminum (2 %) electrolytes are presented in Fig. 1. The cathodic current at –1.2 V observed towards negative potentials is attributed to the zinc cathodic reduction to metal zinc. Judging by the CV curves, an advantage of non-aqueous electrolytes

Table 1. Compositions of zinc DMSO-based electrolytes and applied deposition methods

Sample Name	Electrolyte Composition	Deposition Range, Deposition Pote
Al-0 (Al-0')	0.2 M $Zn(CH_3COO)_2$ 0.5 M KNO_3 0.05 M H_2O_2	–1.6 V (–1.4 V) (–1.8 ÷ –1.2 V) *vs*. Ag/AgCl/KCl(s)
Al-1 (Al-1')	0.2 M $Zn(CH_3COO)_2$ 0.5 M KNO_3 0.05 M H_2O_2 0.0032 M $Al(NO_3)_3$	–1.6 V (–1.8 ÷ –1.5 V) *vs*. Ag/AgCl/KCl(s)
Al-2 (Al-2')	0.2 M $Zn(CH_3COO)_2$ 0.5 M KNO_3 0.05 M H_2O_2 0.0064M $Al(NO_3)_3$	–1.6 V (–1.8 ÷ –1.5 V) *vs*. Ag/AgCl/KCl(s)
Al-4 (Al-4')	0.2 M $Zn(CH_3COO)_2$ 0.5 M KNO_3 0.05 M H_2O_2 0.0128 M $Al(NO_3)_3$	–1.6 V (–1.8 ÷ –1.5 V) *vs*. Ag/AgCl/KCl(s)
Al-6 (Al-6')	0.2 M $Zn(CH_3COO)_2$ 0.5 M KNO_3 0.05 M H_2O_2 0.0192 M $Al(NO_3)_3$	–1.6 V (–1.8 ÷ –1.5 V) *vs*. Ag/AgCl/KCl(s)
Al-10 (Al-10')	0.2 M $Zn(CH_3COO)_2$ 0.5 M KNO_3 0.05 M H_2O_2 0.0256 M $Al(NO_3)_3$	–1.6 V (–1.8 ÷ –1.5 V) *vs*. Ag/AgCl/KCl(s)

originates from no hydrogen release at the cathode below –1.05 V *vs*. Ag|AgCl|KCl(s) [19]. This fact makes the basis for expectation of lower roughness and higher uniformity of the zinc and aluminum coatings deposited in DMSO-based baths.

The coatings produced in electroplating process demonstrated metallic luster. In comparison to the deposits produced in aqueous electrolytes the zinc did not form oxide or oxyhydroxide in electrochemical bath directly [12].

Figure 2 shows MS TG-DTA data for the coating annealing in air. All vapors of the solvent (DMSO) release below 200 °C and the removal of any carbon oxides from organic compounds (including acetate) performed at higher temperatures. At about 360 °C the release of CO_2 is significant but this temperature of annealing does not provide complete removal of carbon from the grey-colored samples. Also, full oxidation of metal zinc to ZnO occurs at higher temperatures only (above 400 °C). For complete transition of zinc compounds to zincite all samples were annealed at 500 °C for 1 h before the following examination. Longer sintering (up to 48 h) at 500 °C showed no changes in phase composition of the samples but resulted in recrystallization and growth of ZnO grain size.

Figure 3 shows the GIXRD data for the coatings annealed at 500 °C. The phase composition of the films corresponds to zincite structure (ICDD PDF-2 Database, file 36-1451) and indium oxide (ICDD PDF-2 Database, file 89-2595) originated from the ITO conductive glass substrate. The most intensive reflections of ZnO are the following (100), (101), (103), (112). The reflection (002) is overlapped with the strong (400) reflection of In_2O_3 phase from ITO substrate. Reflections of any other phases, including metal zinc, are not observed after the thermal treatment.

Most often, high overvoltage results in growth of dendritic deposits. The deposition potential varied in the range of –1.2 ÷ –1.8 V to optimize microstructure of the coatings (Fig. 4).

It is remarkable that the growth of deposition potential up to –1.8 V leads to flake-like zinc and/or

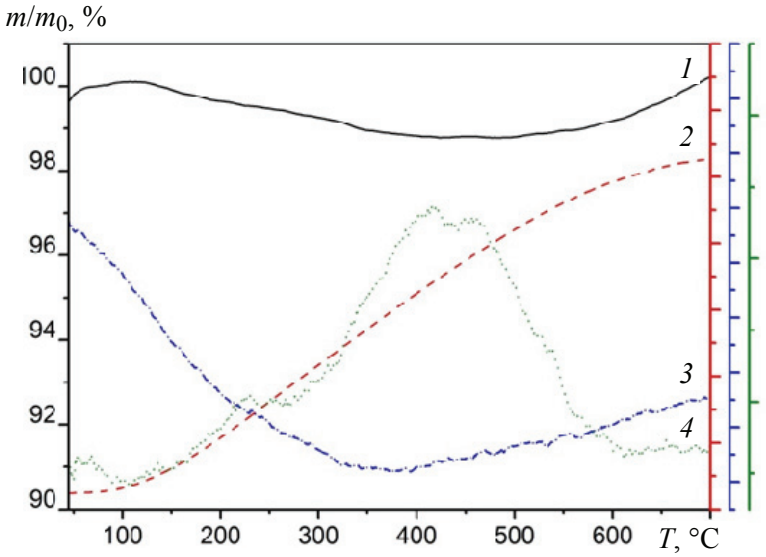

Fig. 2. TG-DTA data for ZnO (Al-0) coatings deposited from DMSO acetate bath at RT before the annealing at 500 °C in air. *1* – weight loss in w%, *2* – DSC effect, *3* and *4* are MS data for release of gas products with mass numbers of 18 and 44, respectively

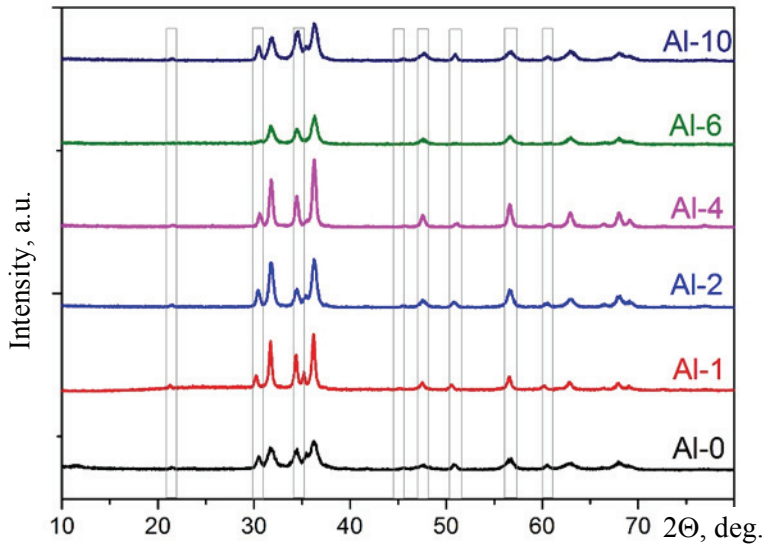

Fig. 3. GIXRD data for ZnO (Al_0) coatings after the annealing at 500 °C in air

ZnO particles which form the porous architecture. For comparison, the coatings obtained from metal zinc deposited under lower overvoltage of –1.2 V show higher uniformity.

The CV curves (see Fig. 1) for the electrolytes with different aluminum content demonstrate an increase of characteristic half-wave potential of the cathodic reduction process. A good matching of the growth rate with a uniformity and dense microstructure with a grain size of about (150 ± 50) nm is achieved at –1.6 V. This deposition potential was used to include much more aluminum in the coating keeping the flat microstructure of the zincite coating.

Figure 4 shows the evolution of microstructure of the coverages with a deposition potential. For the samples deposited at E'_d of –1.2 and –1.4 V the microstructure of ZnO particles is flake-like and particles are partially oriented forming bundles as shown in Fig. 4*b*. The flake-like particles are of 10–20 nm thick and up to 500 nm in lateral dimension. For the ZnO (Al-0) sample deposited at –1.6 V the round shaped particles (D 200 nm) of zincite are observed. At –1.8 V a porous product of disordered ZnO flake-like particle with large pores up

The surface morphology of polycrystalline ZnO(Al) coatings deposited at E_d of –1.6 V demonstrates different particle morphology and aggregate structure and porosity (Fig. 5). According to micrographs, the crystallite size decreases as Al

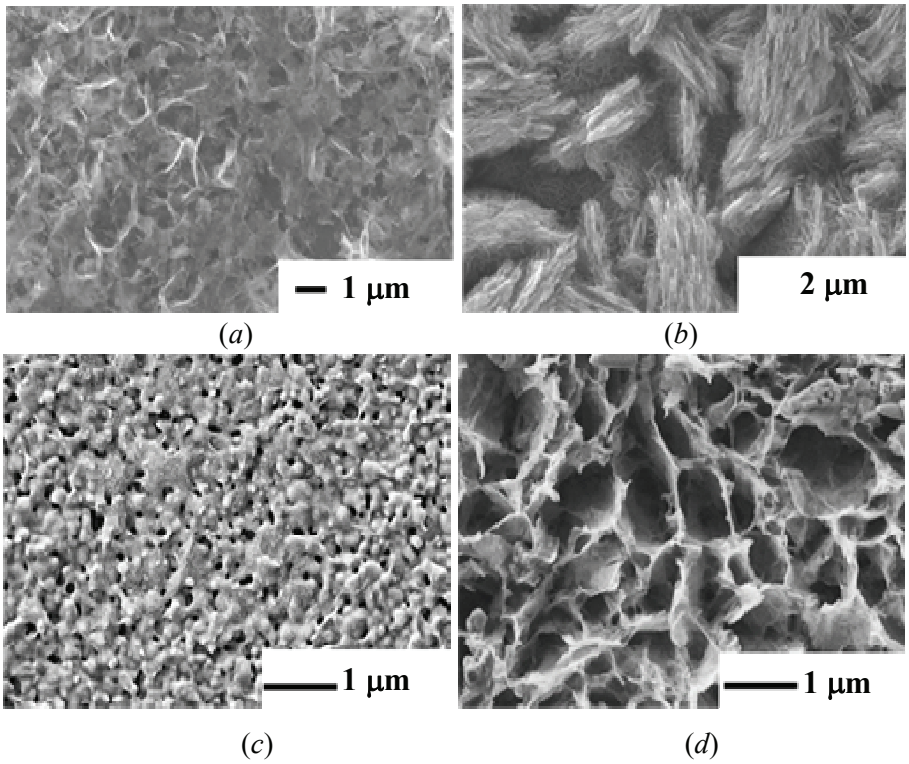

Fig. 4. SEM images data for ZnO coatings deposited using DMSO acetate bath at RT and annealed at 500 °C in oxygen: *a* – –1.2 V; *b* – –1.4 V; *c* – –1.6 V; *d* – –1.8 V

percentage increased that correlates with CV curves (see Fig. 1). The samples Al-6, Al-8, Al-10 show lower crystallinity and complex sponge-like microstructure of thin platelets bended as flakes [12]. This effect could be explained by an increased Al^{3+} capture from electrolytes, decreased current and electrodeposition rates resulting in smaller particles. Thus, the thin flake-like ZnO crystallites (which are typical for ZnO) transform to round-shaped nanocrystallites. At greater overvoltage ZnO crystallites grow faster and forming a very porous deposit of round-shaped particles. The resulting structure is more heterogeneous in thickness, and the coverage itself is more friable and amorphous.

For a series obtained at lower overvoltage of E_d –1.4 V, the presence of two kinds of grains is observed. The first kind is (20 ± 10) nm thick flake-like particles (a lateral size up to 1 – 2 μm) and the second kind is shape-less cohesive material (Fig. 6). The platelets are thinner than their analogues grown under –1.6 V at higher overvoltage. The percentage of thin flake-like particle decreased as Al concentration increased up to 6 at. %. For samples Al-6' and Al-10' the flake-like particles form a composite with different sizes of grains.

The EDX data show a uniform distribution of zinc and aluminum over the surface of the films. The analysis of Al to Zn ratios in the films obtained from DMSO-based electrolytes confirms compliance of the compositions. Aluminum content values are below the estimated values due to the slow diffusion rate of aluminum ions compared to the rate of electrochemical deposition of zinc (Table 2). On the other hand, the EDX data confirm well the effect of an increased aluminum percentage in the sample Al-6 that matches well to XPS data (see Fig. 1).

According to XPS data the percentage of aluminum in the samples correlates to its concentration in electrolyte but higher than expected for Al-6 (Table 2). The increased percentage of Al at the surface proceeded, likely, from segregation of Al because of sintering at 500 °C.

The binding energies of the XPS lines, the kinetic energies of the Auger lines, and the Auger values of the zinc parameter indicate the oxidized state of zinc (Table 3). An analysis of the Al2p line profiles showed the presence of the Al $2p_{3/2}$ and weak Al $2p_{1/2}$ bands in spectra. The binding energy (BE) Al 2p peak centered at 74.10 eV is typical for samples Al-1', Al-2', Al-4', Al-6' (deposited at –1.4 V). It can be related to γ-Al_2O_3 phase [20, 21] observed by XRD above. For samples, prepared at E_d of –1.6 V, the XPS data show the presence of the γ-Al_2O_3 phase with the binding energy (BE) maximum of 74.10 eV for all percentages of Al (Table 3).

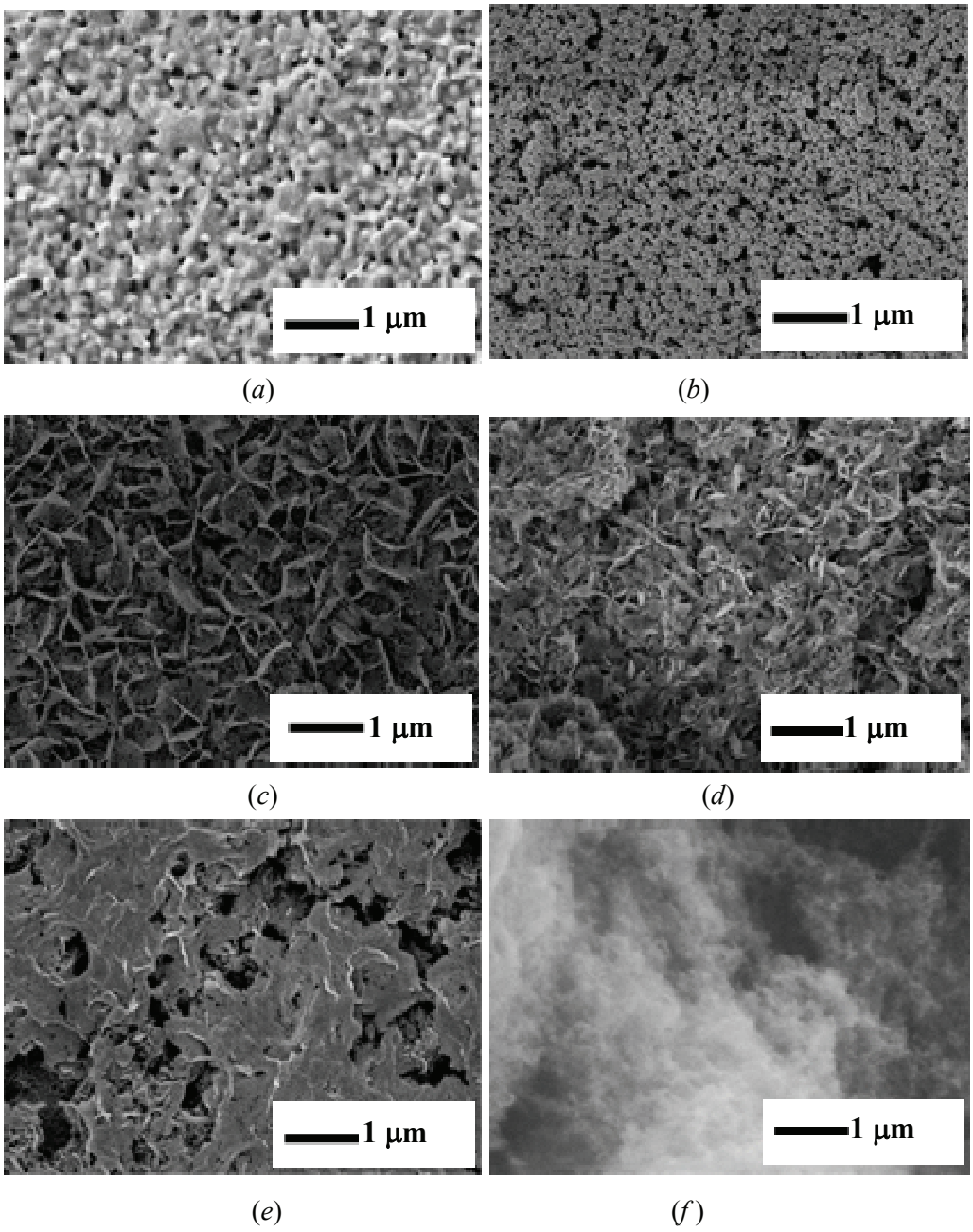

Fig. 5. SEM micrographs ZnO and ZnO(Al) coatings deposited at E_d = –1.6 V from different DMSO acetate electrolytes, namely: *a* – Al-0; *b* – Al-1; *c* – Al-2; *d* – Al-4; *e* – Al-6 and *f* – Al-10

Formation aluminum oxyhydroxide AlOOH (BE = 74.20 eV) and aluminum hydroxide $Al(OH)_3$ (BE of 74.30 eV) [21] admixtures are hardly believable because all syntheses have been performed in DMSO electrolyte.

At the same time, according to *Pelicano et Yanagi* [22] the BE of 73.9 eV could be related to Al substitution of zinc in Zn sublattice of ZnO. The BE of Al $2p_{3/2}$ is close also to a phase of nitride AlN when concentration of Al-1 is low (BE = 73.90 eV). This shift to lower binding energies, probably, corresponds to the structure of AZO while the BE values are higher than for AZO films deposited by magnetron sputtering [23]. The yellowish color of the samples, most likely, originated from any kind of point defects.

At the same time, the XPS data discussed above are related to surface states of the coatings and do not characterize its bulk composition. Also, the limit of the XPS accuracy and low theoretical percentage of Al incorporation to the zuncite make all the speculations above uncertain.

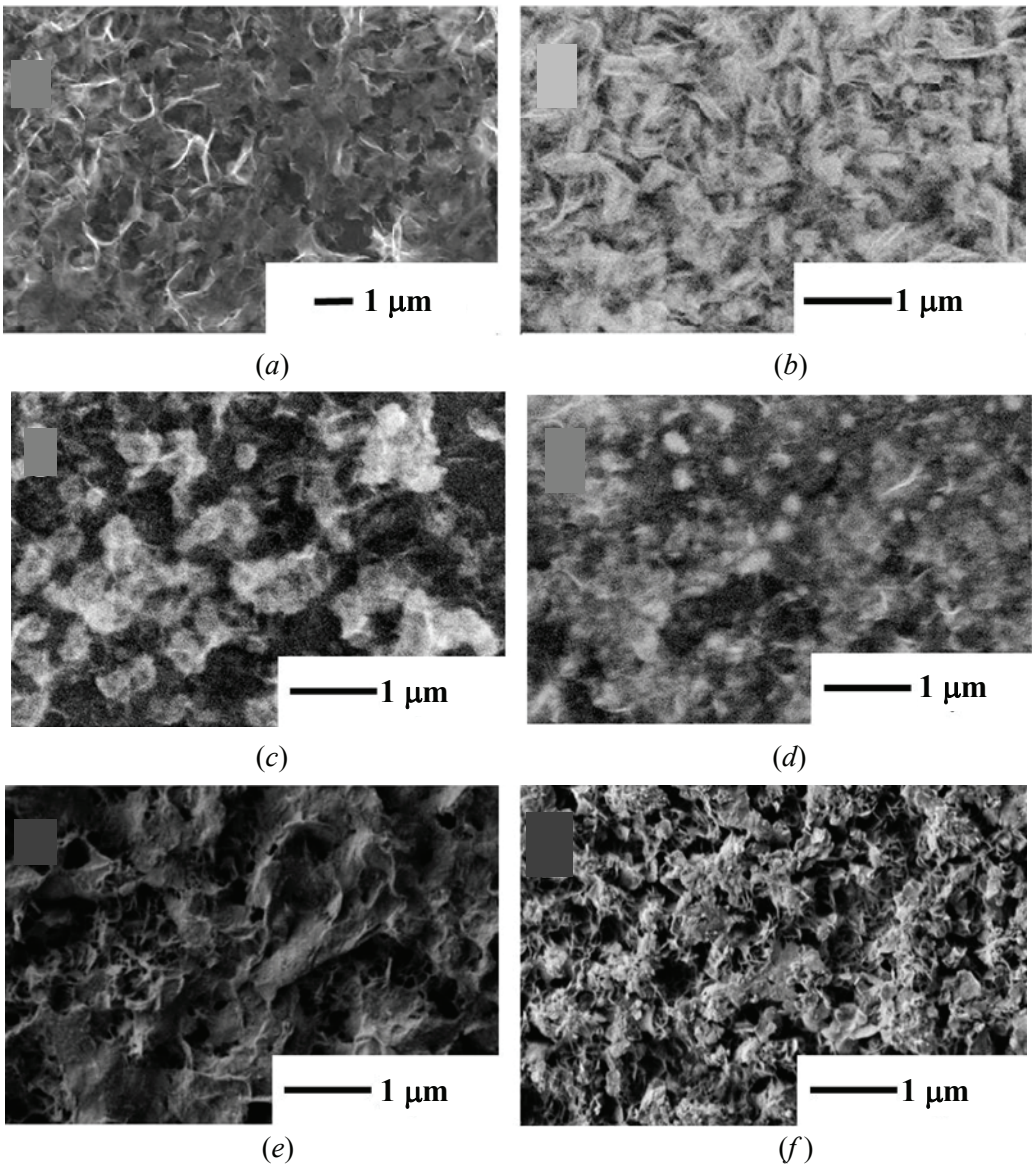

Fig. 6. SEM micrographs ZnO and ZnO(Al) coatings deposited at E_d = –1.4 V from different DMSO acetate electrolytes, namely: *a* – Al-0'; *b* – Al-1'; *c* – Al-2'; *d* – Al-4'; *e* – Al-6' and *f* – Al-10'

Table 2. Characteristics of ZnO(Al) coatings after annealing at 500 °C for 1 hour (1 μm thick coatings analyzed by EDX and XPS)

Samples (methods)	Al/Zn (theory)	Zn (EDX), at. %	Al (EDX), at. %	Al/Zn (EDX)	Zn (XPS), at. %	Al (XPS), at. %	Al/Zn (XPS)
Al-1	0.010	20.4	0.6	0.027	14.3	1.0	0.070
Al-2	0.020	24.7	0.9	0.035	23.0	0.5	0.022
Al-4	0.042	20.7	0.9	0.042	21.2	4.2	0.198
Al-6	0.064	20.0	1.8	0.082	18.1	8.1	0.448
Al-1'	0.010	2.8	0.7	0.26	29.8	2.5	0.084
Al-2'	0.020	2.3	0.6	0.24	25.2	6.3	0.196
Al-4'	0.042	2.7	0.6	0.24	29.2	2.5	0.086
Al-6'	0.064	2.4	0.6	0.20	16.3	9.6	0.589

Table 3. XPS data: binding energy characterization of ZnO(Al) coatings after annealing at 500 °C for 1 h

Samples	Al/Zn (XPS)	$Al2p_{3/2}$	Probable Composition
Al-1	0.070	73.9	ZnO:Al, γ-Al_2O_3
Al-2	0.022	74.1	
Al-4	0.198	74.1	
Al-6	0.448	74.1	
Al-10	0.157	74.1	
Al-1’	0.084	74.2	γ-Al_2O_3
Al-2’	0.250	74.1	
Al-4’	0.086	74.1	
Al-6’	0.589	74.1	
Al-10’	0.188	74.3	

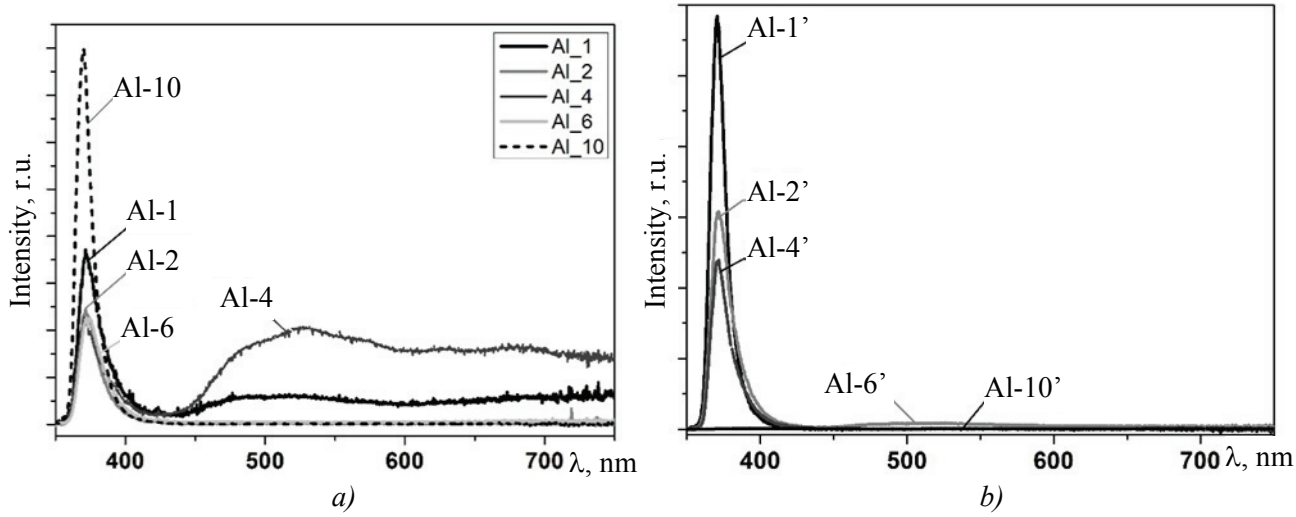

Fig. 7. Photoluminescence spectra of ZnO(Al) coatings, deposited electrochemically from zinc DMSO acetate electrolytes: *a* – samples deposited at –1.6 V; *b* – samples deposited at –1.4 V
(The excitation laser was 337 nm, the spectra collected at 77 K)

The heat treatment conditions are important for characteristic continuity of the films, as well as optimal optical characteristics, and lifetime and mobility of charge carriers. All these characteristics depend on the grain size. The crystalline ZnO coatings are obtained using an acetate nonaqueous electrolyte and then sintered at 500 °C for zincite formation.

Photoluminescence (PL) was applied to analyze the effects of doping on point defects of the zincite (Fig. 7). Pure zinc oxide is characterized by a wide band in the blue, green or yellow spectral region and the exciton peak near the NBE at 385 nm (3.22 eV). Figure shows the room temperature PL spectra of undoped ZnO and ZnO(Al) coverages. As the PL spectra show several bands, the deconvolution of spectrum obtained for the samples deposited at 2 at. % Al electrolyte.

The intensity of 377 nm may be due to the bandwidth transition, the intensity of 385 nm (3.22 V) may be due to free exciton recombination and is close to electron-hole recombination from the bottom of conduction band to the top of the valence band. An increase in the total intensity is observed up to a concentration of 4 at. % Al.

Generally, luminescence properties of the thin films have a close relation with crystallinity because the density of defects reduces with an improvement of the crystallinity. Thus, intensity of the UV emission of ZnO films is dependent on the microcrystalline structure and stoichiometry, which is in agreement with the XRD results. The energy levels of intrinsic defects in ZnO were calculated by applying full-potential linear muffin-tin orbital method and the results are presented in [24].

The peak at about 530 nm is due to the radiative recombination of a photogenerated hole in the valence band with an electron occupying the deep oxygen vacancy energy band. The undoped ZnO film shows a very broad feature below 530 nm due to the presence of interstitial oxygen defects in ZnO film.

The obtained ZnO(Al) coatings have been characterized by a high transmittance in the visible range. The 300 nm – thick coverages the light transmission values are in the range of 85–90 at. % 550 nm in the case of 4–6 at. % of Al content.

4. Conclusion

The electrochemical co-precipitation of zinc and aluminum using DMSO-based acetate electrolytes with the following oxidation is a promising method for double-oxide coating formation. The method requires an accurate post-deposition thermal treatment in oxidative atmosphere to reach zinc and aluminum oxides. The thermal oxidation of metal by molecular oxygen performed at 500 °C for 1 h could be substituted by other mild and inexpensive technique to prevent segregation of alumina. There are also no noticeable changes in the lattice parameter of zincite with aluminum content, probably, as a result of inaccuracy of XRD data refinement, because the expected growth of parameters is only 1–2 % of the unit cell value. On the other hand, the analysis of Al $2p_{3/2}$ band in XPS spectra and photoluminescence spectroscopy data could be interpreted as a deficiency growth in ZnO lattice including aluminum in zinc sublattice of ZnO. The formation of γ-Al_2O_3 is observed by XPS only while according to XRD data no separate phase of alumina is present. This means that crystallites of alumina are nano-sized, and could be a product of a segregation or oxidation of fine and evenly diffused aluminum particles.

5. Funding

This project is supported by the Russian Science Foundation, grant No. 22-23-00585.

6. Acknowledgements

The authors are grateful to the colleagues from Lomonosov Moscow State University Dr. Olga V. Boytsova, Dr. Kh. E. Yorov for their assistance in SEM experiments.

The project was performed using the equipment of the collective resource center of Moscow State University “Technologies for synthesis of new nanostructured materials and their complex characterization”.

The authors acknowledge support from Lomonosov Moscow State University Program of Development for providing access to the XPS facility.

7. Conflict of interests

The authors declare no conflict of interest.

References

1. Wang H, Li K, Tao Y, Li J, Li Y, et al. Smooth ZnO:Al - AgNWs composite electrode for flexible organic light- emitting device. *Nanoscale Research Letters.* 2017;12(77):1-7. DOI:10.1186/s11671-017-1841-2

2. Lee S-H, Han S-H, Jung HS, Shin H, Lee J, et al. Al-doped ZnO thin film: a new transparent conducting layer for ZnO nanowire-based dye-sensitized solar cells. *Journal of Physical Chemistry C.* 2010;114:7185-7189. DOI:10.1021/jp1008412

3. Treharne RE, Hutchings K, Lamb DA, Irvine SJC, Lane D, Durose K. Combinatorial optimization of Al-doped ZnO films for thin-film photovoltaics. *Journal of Physics D: Applied Physics.* 2012;45:335102(1-8). DOI:10.1088/0022-3727/45/33/335102

4. Pathirane MK, Khaligh HH, Goldthorpe IA, Wong WS. Al-doped ZnO/Ag-nanowire composite electrodes for flexible 3-dimensional nanowire solar cells. *Scientific Reports.* 2017;7:1-7. DOI:10.1038/s41598-017-07180-1

5. Li X, Ye W, Zhou X, Huang F, Zhong D. Increased efficiency for perovskite photovoltaics based on aluminum-doped zinc oxide transparent electrodes via surface modification. *Journal of Physical Chemistry C.* 2017;121:10282-10288. DOI:10.1021/acs.jpcc.7b00419

6. Pradhan AK, Mundle RM, Santiago K, Skuza JR, Xiao BS, et al. Extreme tunability in aluminum doped zinc oxide plasmonic materials for near-infrared applications. *Scientific Reports.* 2014;4:19-21. DOI:10.1038/srep06415

7. Rahman BMA, Bhattacharjee R, Kejalakshmy NT. Design and optimization of an Al doped ZnO in Si-slot for gas sensing design and optimization of an Al doped ZnO in Si-slot for gas sensing. *IEEE Photonics Journal.* 2018;10(4):1-10. DOI:10.1109/JPHOT.2018.2849383

8. Baruah A, Jindal A, Acharya C. Microfluidic reactors for the morphology controlled synthesis and photocatalytic study of ZnO nanostructures. *Journal of Micromechanics and Microengineering.* 2017;27:035013 (1-6). DOI:10.1088/1361-6439/aa5bc4

9. Azzouz I, Habba YG, Capochichi-Gnambodoe M, Marty F, Vial J. Zinc oxide nano-enabled microreactor for water purification and its applicability to volatile organic compounds. *Microsystems & Nanoengineering.* 2018;4:17093(1-7). DOI:10.1038/micronano.2017.93

10. Gerstl M, Hutterer A, Fleig J, Bram M, Karl A. Model composite microelectrodes as a pathfinder for fully oxidic SOFC anodes. *Solid State Ionics.* 2016;298:1-8. DOI:10.1016/j.ssi.2016.10.013

11. Pullini D, Pruna A, Zanin S, Mataix DB. High-efficiency electrodeposition of large scale ZnO nanorod arrays for thin transparent electrodes. *Journal of the Electrochemical Society.* 2011;159(2):45-51. DOI: 10.1149/2.093202jes

12. Martynova NA, Svishchev VN, Lepnev LS, Alieva SR, Chertorylskaya EG, et al. Electrochemical coprecipitation of zinc and aluminum in aqueous electrolytes for ZnO and AZO coverage deposition. *International Journal of Photoenergy*. 2019;6808347(1-10). DOI:10.1155/2019/6808347

13. Hirahara N, Onwona-Agyeman B, Nakao M. Preparation of Al-doped ZnO thin films as transparent conductive substrate in dye-sensitized solar cell. *Thin Solid Films.* 2012;520(6):2123-2127. DOI:10.1016/ j.tsf.2011.08.100

14. Gal D, Hodesa G, Lincot D, Schock H-W. Electrochemical deposition of zinc oxide films from non-aqueous solution: a new buffer/window process for thin film solar cells. *Thin Solid Films.* 2000;361-362:79-83. DOI:10.1016/S0040-6090(99)00772-5

15. Tello A, Gomez H, Munoz E, Riveros G, Pereyra CJ, et al. Electrodeposition of nanostructured ZnO thin films from dimethylsulfoxide solution: effect of temperatures on the morphological and opptical properties. *Journal of the Electrochemical Society.* 2012;159(12):750-755. DOI:10.1149/2.017301jes

16. Riveros G, Ramírez D, Tello A, Schrebler R, Henríquez R, Gómez H. Electrodeposition of ZnO from DMSO solution: Influence of anion nature and its concentration in the nucleation and growth mechanisms. *Journal of the Brazilian Chemical Society.* 2012;23(3): 505-512. DOI:10.1590/S0103-50532012000300018

17. Kang D, Lee D, Choi K-S. Electrochemical synthesis of highly oriented, transparent, and pinhole-free ZnO and Al-doped ZnO films and their use in heterojunction solar cells. *Langmuir.* 2016;32:10459-10466. DOI:10.1021/acs.langmuir.6b01902

18. Liang Y-C. Microstructure and optical properties of electrodeposited Al-doped ZnO nanosheets. *Ceramics International.* 2012;38:119-124. DOI:10.1016/j.ceramint. 2011.05.154

19. Hsu P-C, Seol S-K, Lo T-N, Liu C-J, Wang C-L, et al. Hydrogen bubbles and the growth morphology of ramified zinc by electrodeposition. *Journal of the Electrochemical Society.* 2008;155(5):400-407. DOI:10.1149/1.2894189

20. Wagner CD, Passoja DE, Hillery HF, Kinisky TG, Six HA, et al. Auger and photoelectron line energy relationships in aluminum–oxygen and silicon–oxygen compounds. *Journal of Vacuum Science and Technology.* 1982;21(4)933-944. DOI:10.1116/1.571870

21. Okamoto Y, Imanaka T, Teranishi S. Surface structure and catalytic activity of MoO_3/Al_2O_3 catalysts in the hydrodesulfurization of thiophene studied by X-ray photoelectron spectroscopy. *Journal of Catalysis.* 1980;65(2):448-460. DOI:10.1016/0021-9517(80)90322-X

22. Pelicano CM, Yanagi H. Enhanced charge transport in Al-doped ZnO nanotubes designed via simultaneous etching and Al doping of H_2O-oxidized ZnO nanorods for solar cell applications. *Journal of Materials Chemistry C.* 2019;7(16):4653-4661. DOI:10.1039/ C9TC00401G

23. Yao P-C, Hang S-T, Wu M-J. Growth characteristics and properties of Al-doped ZnO thin films by DC magnetron sputtering from AZOY® target. *Transactions of the Canadian Society for Mechanical Engineering.* 2013;37(3):303-312. DOI:10.1139/tcsme-2013-0020

24. Thandavan TM, Gani SM, Wong CS, Nor RM. Enhanced photoluminescence and Raman properties of Al-Doped ZnO nanostructures prepared using thermal chemical vapor deposition of methanol assisted with heated brass. *PloS One.* 2015;10(5):0126189(1-18). DOI:10.1371/journal.pone.0121756

Information about the authors / Информация об авторах

Natalia A. Martynova, Cand. Sc. (Chem.), Lomonosov Moscow State University (MSU), Moscow, Russian Federation; ORCID 0000-0003-3529-6561; e-mail: natalia.nn21@gmail.com

Мартынова Наталья Александровна, кандидат химических наук, Московский государственный университет имени М.В. Ломоносова (МГУ имени М.В. Ломоносова), Москва, Российская Федерация; ORCID 0000-0003-3529-6561; e-mail: Natalia.nn21@ gmail.com

Leonid S. Lepnev, D. Sc. (Phys. and Math.), High-Qualified Leading Senior Researcher, P.N. Lebedev Physical Institute of the Russian Academy of Sciences (LPI RAS), Moscow, Russian Federation; ORCID 0009-0008-1363-0761; e-mail: llepn@mail.ru

Лепнев Леонид Сергеевич, доктор физико-математических наук, высококвалифицированный ведущий научный сотрудник, Физический институт имени П. Н. Лебедева РАН, Москва, Российская Федерация; ORCID 0009-0008-1363-0761; e-mail: llepn@ mail.ru

Dmitry M. Tsymbarenko, Cand. Sc. (Chem.), Senior Researcher, MSU, Moscow, Russian Federation; ORCID 0000-0002-2818-5639; e-mail: tsymbarenko@gmail.com

Konstantin I. Maslakov, Cand. Sc. (Phys.-Math.), Senior Researcher, MSU, Moscow, Russian Federation; ORCID 0000-0002-0672-2683; e-mail: nonvitas@gmail.com

Tatiana B. Shatalova, Cand. Sc. (Chem.), Associate Professor, MSU, Moscow, Russian Federation; ORCID 0000-0002-4304-8624; e-mail: shatalova@inorg.chem.msu.ru

Serguei V. Savilov, D. Sc. (Chem.), Leading Senior Researcher, MSU, Moscow, Russian Federation; ORCID 0000-0002-5827-3912; e-mail: savilov@mail.ru

Anastasia V. Grigorieva, Cand. Sc. (Chem.), Associate Professor, MSU, Moscow, Russian Federation; ORCID 0000-0001-6102-9024; e-mail: anastasia@inorg.chem.msu.ru

Цымбаренко Дмитрий Михайлович, кандидат химических наук, старший научный сотрудник, МГУ имени М.В. Ломоносова, Москва, Российская Федерация; ORCID 0000-0002-2818-5639; e-mail: tsymbarenko@gmail.com

Маслаков Константин Игоревич, кандидат физико-математических наук, старший научный сотрудник, МГУ имени М.В. Ломоносова, Москва, Российская Федерация; ORCID 0000-0002-0672-2683; e-mail: nonvitas@gmail.com

Шаталова Татьяна Борисовна, кандидат химических наук, доцент, МГУ имени М. В. Ломоносова, Москва, Российская Федерация; ORCID 0000-0002-4304-8624; e-mail: shatalova@inorg.chem.msu.ru

Савилов Сергей Вячеславович, доктор химических наук, ведущий научный сотрудник, МГУ имени М.В. Ломоносова, Москва, Российская Федерация; ORCID 0000-0002-5827-3912; e-mail: savilov@mail.ru

Григорьева Анастасия Вадимовна, кандидат химических наук, доцент, МГУ имени М. В. Ломоносова, Москва, Российская Федерация; ORCID 0000-0001-6102-9024; e-mail: anastasia@inorg.chem.msu.ru

Received 10 January 2023; Accepted 02 March 2023; Published 26 May 2023